Assimilation of Satellite Imager Data and Surface Observations to Improve Analysis of Circulations Forced by Cloud Shading Contrasts

FRANK H. RUGGIERO

Battlespace Environment Division, Air Force Research Laboratory, Hanscom Air Force Base, Massachusetts

GEORGE D. MODICA AND ALAN E. LIPTON

Atmospheric and Environmental Research, Inc., Cambridge, Massachusetts

(Manuscript received 14 September 1998, in final form 27 January 1999)

ABSTRACT

An assimilation system that performs continuous assimilation of satellite imager data and intermittent assimilation of hourly surface observations is described. The system was applied to a case study of the southeast United States that was heavily influenced by the shading effect of an area of morning stratiform clouds. The results of analyses produced during the assimilation show improvement in the depiction of the modified surface heating effects beneath the cloudy region as well as in important convective precursors such as mass and moisture convergence and convective available potential energy in the cloudy and adjoining regions. Without assimilation of these data, the numerical model was less able to simulate these thermally forced circulations.

1. Introduction

The prediction of locally forced convective clouds is a significant nowcasting problem for certain areas of the United States. Purdom and Marcus (1982) have pointed out, for example, that most of the morning and early afternoon summertime convection that occurs in the southeastern United States is predominantly locally driven. One of the primary drivers of locally forced convection is differential surface heating, which causes adjustments to the wind field that result in local areas of convergence. Mechanisms for generating differential surface heating include land–sea interfaces (e.g., Byers and Braham 1949; Burpee 1979), differential vegetation patterns (Rabin et al. 1990; Hong et al. 1995), topography (Toth and Johnson 1985; Abbs and Pielke 1986), and differential cloud shading (Bailey et al. 1981; Segal et al. 1986, 1993).

The objective of this paper is the development of a hybrid assimilation system to improve the diagnosis of convective initiation due to differential cloud shading. In cloudy areas, reduction of surface insolation leads to decreased surface heating, decreased sensible heat transfer from the surface to the atmosphere, and depression of near-surface air temperatures. These effects can play a major role in determining where and when deep convection will develop. Local contrasts in convective destabilization may occur when one region is cloud covered and an adjacent region is clear. Circulations analogous to sea breezes may develop, with subsidence and outflow occurring in cooler, cloud-shaded regions while rising motion and inflow occur in nearby warmer regions (Segal et al. 1986). Bailey et al. (1981) provided an example of cloud-shading contrasts and demonstrated their critical importance for the forecast of a convective rainstorm.

In trying to predict the potential for circulations generated by differential cloud shading (or other local forcing), the standard synoptic upper-air radiosonde network is of limited use given its coarse temporal and spatial resolutions. Hourly surface observations provide improved temporal and spatial resolution and have been shown to accurately depict mesoscale features (Miller and Benjamin 1992; Ruggiero et al. 1996). However, the spatial resolution of the surface observation sites is still not dense enough to adequately resolve cloud-shading contrasts in some situations.

Another useful source for monitoring cloud effects is geostationary satellite imagers, which can take data frequently enough to track the evolution of cloud fields, particularly when the clouds are stratiform. Horizontal spatial resolutions as fine as 1 km are available. Geostationary satellite visible imagers do not cover the entire spectrum of solar energy (Menzel and Purdom 1994), but their spectral response is broad enough to make it possible to infer insolation from their data

Corresponding author address: Dr. Frank H. Ruggiero, AFRL/VSBL 29 Randolph Rd., Hanscom AFB, MA 01731-3010.
E-mail: ruggiero@plh.af.mil

TABLE 1. Features of the NCAR–PSU Mesoscale Model.

Horizontal grid	Arakawa ''B'' grid; 50 × 55, 45 km (outer grid) and 67 × 85, 15 km (nested grid)
Vertical grid	Staggered; variable resolution, σ coordinate; 28 levels
Boundary layer	High resolution; K-theory with nonlocal plume model for unstable regime (Zhang and Anthes 1982)
Cumulus convection	Modified Kuo (Anthes 1977)
Initial condition	Standard surface and rawinsonde data from 0700 EST (1200 UTC) 23 Aug 1993; successive-corrections objective analysis with NCEP global analysis as first guess (Benjamin and Seaman 1985); implicit normal model initialization (Errico and Bates 1988)

(Schmetz 1989). An effort to retrieve cloud radiative characteristics from geostationary satellite data and assimilate the data into a mesoscale model was reported by Lipton (1993), who used a time-continuous approach that ensures that the modeled cloud effects are consistent with observations over an extended time. During assimilation, the modeled solar heating, thermally forced circulations, and destabilization patterns evolve in response to the effects of the observed cloud cover. The value of the method for mesoscale analysis was demonstrated in simulations and in a case study in the Texas panhandle area. McNider et al. (1995) used a similar assimilation method to study the same case. Both studies found that assimilation had a large impact on gradients of near-surface temperatures and the depth of the boundary layer and a significant impact on mesoscale circulations.

To accomplish the paper's objective, data from the Geostationary Operational Environmental Satellite (GOES) imager and hourly reporting surface stations were employed. The satellite imager data assimilation was carried out in the time-continuous fashion following the method developed by Lipton (1993). The method works by using visible image data to improve the model's computation of solar heating in the surface energy budget. The hourly surface observations were assimilated intermittently as described by Ruggiero et al. (1996). This method includes a technique to vertically blend the surface observation analysis increments at the model's lowest sigma level to other model levels within the model's planetary boundary layer. These two data sources are both readily available in the continental United States throughout the morning and early afternoon preconvective period and are highly complementary to each other. The satellite visible imager is one of the few sources of data that can provide information on domains and resolutions commensurate with mesoscale models. Hourly reporting surface stations have coarser horizontal resolution, but they provide direct observations within the boundary layer, without the sources of error that are inherent to indirect retrievals from remote sensors.

2. Assimilation system

a. Model description

The model used for this study was the National Center for Atmospheric Research–Pennsylvania State University (NCAR–PSU) Mesoscale Model 4 (MM4) version 8. The primary relevant features of this model are listed in Table 1. The model was run in nested mode and all the results presented here are for the nested grid.

Of fundamental importance in depicting surface thermal gradients is knowledge of how the model computes ground surface temperatures. The MM4 holds ocean surface temperatures constant using values from the National Centers for Environmental Prediction (NCEP) global analysis. Over land, the MM4 computes surface temperatures using a prognostic surface energy budget equation that includes terms representing the sensible and latent heat fluxes to the atmosphere, sensible heat flux into the soil, and solar and infrared radiative fluxes (Zhang and Anthes 1982). The MM4 formulation accounts for cloud effects on surface radiation by way of fractional cloud cover parameters n_i that are computed solely on the basis of the relative humidity field. The subscript *i* refers to the three layers of cloud represented in the model 1) low, 2) middle, and 3) high. The solar transmittance of a cloudy atmosphere is computed as a simple function of n_i (Benjamin 1983).

b. Satellite imager data assimilation

The method employed in this study for retrieving and assimilating cloud radiative effects from satellite imager data is, in many respects, similar to the one reported in Lipton (1993). The method involves retrieving from satellite image data the effective solar transmittances and infrared emittances over cloudy areas within the domain, and then assimilating that information into the model computations of surface downwelling radiation. The use of the MM4 as assimilating mesoscale model is a change from the system reported in Lipton (1993). The mesoscale model used previously was unable to represent synoptic-scale weather features and represented only features imposed through satellite data assimilation or

forced by terrain inhomogeneities. A brief review of the method is given below and is followed by a description of the changes made to accommodate the inclusion of the NCAR–PSU MM4.

The effective solar transmittance, τ_{eff}, is computed by adapting the method that Gautier et al. (1980) and Diak and Gautier (1983) developed for computing insolation at the ground surface from GOES visible imager data. The method is optimized for middle and low-level liquid water clouds, which are responsible for the bulk of shading effects in many situations. The two major steps of their method are retrieval of the cloud reflectance (A_c) and absorptance (abs) from the image data and computation of the surface insolation using a simple radiative transfer model. By revising their formulation, the impact of clouds on insolation was separated as a multiplicative term of the form

$$SW_{\downarrow\text{cloudy}} = SW_{\downarrow\text{clear}}\,[(1 - A_c - \text{abs})(1 + A_s A_c)], \quad (1)$$

where $SW_{\downarrow\text{clear}}$ is the downward shortwave radiation (insolation) at the surface under a cloud-free assumption and A_s is the broadband albedo of the ground surface, which was assumed to be 0.16. The rightmost term in parentheses represents radiation that penetrates the cloud, is reflected by the ground, and is then reflected back to the ground by the cloud base. To determine the effective solar transmittance for a mesoscale model grid box (τ_{eff}), the bracketed term in (1) is computed at each image pixel within the grid box, and the resulting values are averaged.

The effective infrared emittance is estimated using an adaptation of the Stephens (1978; Stephens et al. 1984) method for parameterizing radiation in water clouds. The Stephens formulation for computing solar reflectance from integrated cloud liquid water (W) is inverted, so that W is computed from A_c. Then the Stephens infrared formulation is used to compute the cloud infrared emittance from W. The result of the Stephens formula is adjusted to take account of uncertainties in fractional cloud cover within a satellite pixel, to arrive at an ''effective'' infrared emittance. The retrieved effective emittance values at all pixels in a mesoscale model grid box are averaged to obtain the grid-scale value, ε.

When used in computations of downwelling surface radiation, the satellite-retrieved values of τ_{eff} and ε at each mesoscale model grid point must be temporally interpolated between satellite observation times. The values are needed at every time step (at intervals of 20 s, in this case), while images have typically been obtained and analyzed at intervals of 1 h. The interpolations are done using a semi-Lagrangian advection scheme to account for cloud movement between image times, where clouds are assumed to move with the vertically averaged lower-tropospheric winds.

A change was required in the assimilation procedure to accommodate the grid nesting employed in our MM4 experiments but not in previous experiments. In the experiments discussed below, values of τ_{eff} and ε were retrieved for the entire nested grid area and applied to the nested grid and the portion of the coarse grid that overlapped the nested grid. The coarse-grid model area outside of the nested grid area was assumed to be cloud free (using clear-sky values of τ_{eff} and ε). This assumption was made to avoid the computational expense and other complications involved in making cloud retrievals over the entire coarse grid or executing different cloud radiation methods in different parts of the grid simultaneously.

The MM4 version of the satellite data assimilation works by altering the MM4 to compute the solar flux in cloudy areas from

$$Q_{s(\text{cloudy})} = Q_{s(\text{clear})}\,\tau_{\text{eff}}, \quad (2)$$

where $Q_{s(\text{clear})}$ is the insolation computed by the model's ordinary radiation parameterization for clear skies. In addition, the effective infrared emittance values are used to adjust the values of n, using a multiplier on n_1, n_2, and n_3 to constrain them to fit the relation $n_1 + n_2 + n_3 = \varepsilon$ (an assumption of zero cloud overlap). We chose to make only this minor modification to the MM4 infrared formulation because, while the formulation is far from the state of the art, we considered it to be adequate for this study since infrared forcing was of secondary importance, relative to solar forcing.

An additional minor modification to the assimilation method was made to account for the effects of boundary-layer aerosols on insolation. A substantial haze was apparent in the satellite images over most of the analysis domain—a condition that is consistent with the high surface dewpoint temperatures (Peterson et al. 1981). The impact of the aerosols on insolation was estimated by comparing clear-sky MM4 computations of insolation with surface pyranometer observations (Hanson and Stoffel 1989). The ratio of the observed insolation to the MM4-computed value can provide a rough estimate of the aerosol-layer transmittance (for direct and diffuse radiation combined). There were far too few available observations to make any reasonable estimate of the horizontal or temporal variability of the aerosol effect, considering that comparisons could be made only if the observation site appeared to be completely cloud-free in a concurrent satellite image. Data from South Carolina State University, which was the pyranometer station closest to the area of primary interest, indicated an aerosol transmittance of 0.91. This value is within the range of those deduced from summertime observations around St. Louis, Missouri (Method and Carlson 1982). As a first-order means to account for the aerosols, this transmittance value was used as a constraint, such that $\tau_{\text{eff}} \leq 0.91$ throughout the domain. Likewise, in control experiments without satellite data assimilation, the computed insolation was constrained by $0.91\ Q_{s(\text{clear})}$.

The mesoscale assimilation system includes an option to augment the assimilation of cloud radiative parameters retrieved from visible image data with the assim-

ilation of data from an infrared satellite sounder (Lipton 1993; Lipton and Vonder Haar 1990; Lipton et al. 1995). With this option data from the two sources are combined in the computation of model surface temperatures. The option was not employed for this study because, on the day being studied, the usual satellite sounder coverage of the southeast United States was preempted by special operations of the satellite instruments. While a more accurate analysis may be achievable with the inclusion of sounder data, an evaluation of the cloud-shading effect is not substantially hindered by the absence of sounder data.

The assimilation data used in this study were from the GOES-7 Visible and Infrared Spin Scan Radiometer, which had the ability to take image data in one visible band and in several infrared bands. The visible data were taken at a nominal ground resolution of 1 km. Seven image datasets, taken hourly over the period of 0700–1300 EST 23 August 1993, were obtained from the archives of the University of Wisconsin Space Science and Engineering Center.

The image data were processed to diminish the striping that results from variations in responsiveness of the visible radiation detectors as they scan across the earth (Lipton 1993; Weinreb et al. 1989). It was also necessary to calibrate the data because, for *GOES-7* and previous GOES satellites, the visible channel data were not automatically calibrated. The calibration procedure used was the same as in Lipton (1993) but referenced to pyranometer data from a station at South Carolina State University.

The cloudy areas of each hourly image were identified and flagged using a person–computer interactive cloud-clear discrimination program on the Air Force Research Laboratory Interactive Meteorological System. Infrared image data were used along with the visible data for this process. The cloud flags were made so that retrieval of cloud radiative parameters could be restricted to areas that were identified as cloudy.

c. Surface data assimilation

The surface observations were assimilated via intermittent assimilation in which a regular cycle of analysis and model integration was carried out. The objective analysis of the surface data was accomplished by the successive correction scheme of Bratseth (1986) as adapted by Ruggiero et al. (1996). The surface data analysis is univariate and performed on the model's lowest computed sigma layer. Before the analysis begins, corrections are made to the observations to adjust for height differences between the model's lowest sigma-level grid points and the observations. After the analysis is complete, the deviations from the first guess at the model's lowest sigma layer are dynamically blended in the vertical with other model layers following the turbulent mixing-based scheme outlined in Ruggiero et al. (1996).

For this work, some modifications were made to the method of Ruggiero et al. (1996). First, the correction to the observed temperature to account for height differences was improved. The method was designed to be consistent with the MM4 formulation for the surface heat flux (Blackadar 1979). In the adjustment method, the surface-layer friction temperature (T_*) is assumed to be constant throughout the model's lowest layer. Therefore,

$$T_* = \frac{\theta_a - \theta_g}{\ln\frac{z_a}{z_0} - \Psi_a} = \frac{\theta_s - \theta_g}{\ln\frac{z_s}{z_0} - \Psi_s}, \tag{3}$$

where θ is the potential temperature; z_0 is the roughness length; z is the height; Ψ is a height-dependent, nondimensional stability parameter; and the subscripts a, s, and g refer to the middle of the lowest sigma layer, shelter height, and ground, respectively. The ground temperature, θ_g, is extracted from the model's surface energy budget equation. Assuming that θ_g remains constant during an objective analysis step, an estimated value of θ_a based on the observed θ_s can be computed iteratively from the relationship on the right side of Eq. (3) by

$$\theta_a^{i+1} = (\theta_s - \theta_g)\frac{\left(\ln\frac{z_a}{z_0} - \Psi_a^i\right)}{\left(\ln\frac{z_s}{z_0} - \Psi_s^i\right)} + \theta_g, \tag{4}$$

where i represents the ith iteration.

In addition to being more physically consistent with the model physics, this new vertical adjustment procedure for temperature is also compatible with the satellite imager data assimilation. Since the imager data improves the model's representation of insolation, it tends to result in improved ground temperatures. The above method makes use of the ground temperature and thus provides a physical tie between the two data sources.

Another change to the procedure of Ruggiero et al. (1996) was the method of prescribing the observed and background error variances. Previously, the error values were based on observed error and forecast error growth statistics generated from other models. A drawback to that approach was that the observation error was used in place of the analysis error when estimating the background error. Using the observation error for the analysis error led to a larger background error computation than when using an explicitly computed analysis error. Furthermore, statistics generated from other models could not possibly provide an adequate depiction of the changes in background error during the course of assimilation, where the background should improve each time data are assimilated. For this work, the observed and background error variances were computed at each

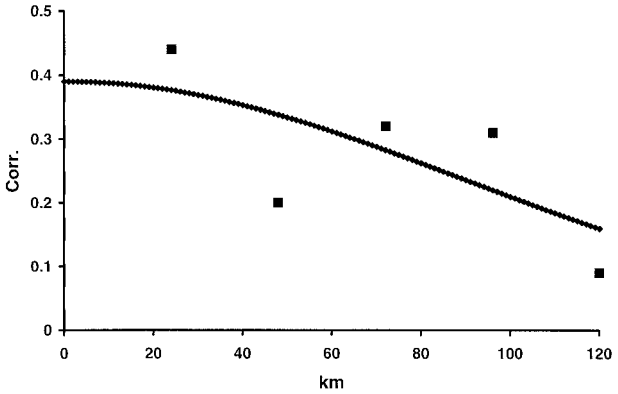

FIG. 1. Horizontal correlations of observation minus background values for each distance of 24 km at 0900 EST 23 Aug 1993 for temperature. The heavy dotted line represents the Gaussian best-fit curve for the correlations.

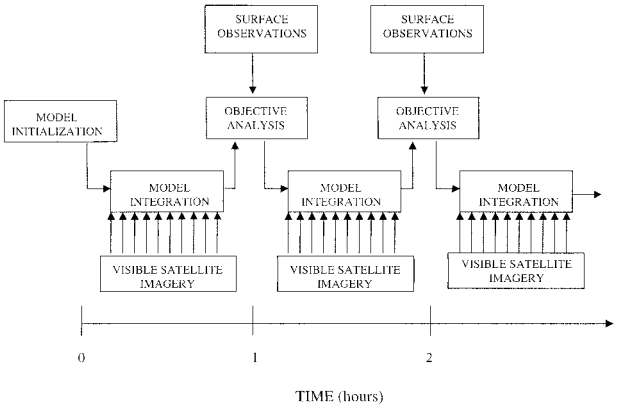

FIG. 2. Schematic of the combined assimilation of satellite imager and surface observation data.

analysis time using a procedure outlined in Daley (1991, 111–114).

The method described by Daley was adapted as follows and was applied at each hour of the analysis. Increments of observation minus background values were computed at each observation site. Horizontal correlations of the increments were computed by binning all possible pairs of observation sites according to the distance between the sites, yielding one correlation value for each distance bin. A Gaussian curve was fit by least squares to the correlations as a function of distance, with an intercept at R_z. An example for temperature at 0900 EST is given in Fig. 1. Then the background error variances (E_B^2) and observation error variances (E_O^2) were computed from $E_B^2 = R_z E_I^2$ and $E_O^2 = E_I^2 - E_B^2$, respectively, where E_I^2 is the variance of the increments. A potential problem is that the procedure is designed to be used with independent data, whereas in this case we were using the same data to estimate the error variances as were used in the analysis. While this approach is not robust, there is no real solution to this problem other than running the model and assimilation package over hundreds of cases to generate the required statistics. For exploratory research, numerous runs are simply not feasible and robustness is not of primary importance.

The last major departure from the Ruggiero et al. (1996) method was the omission of model initialization following the analysis update steps in the assimilation cycle. In the previous work, the most frequently the surface data assimilation was carried out was 3 h. In this work, the assimilation was carried out hourly and we expected that including a balance-based initialization at each hour would greatly hinder the model's ability to develop its divergence fields, which were a focus of this work.

The merger of the surface and satellite assimilation methods is shown schematically in Fig. 2. The figure displays a two-cycle intermittent assimilation of the surface observations along with continuous assimilation of satellite imager data.

3. Experiment design

The synoptic situation for this case study has been discussed by Lipton and Modica (1999) and will be briefly summarized here. The case is from 23 August 1993 and encompasses the southeast United States. On that morning, stratiform clouds covered a broad region from central Georgia to western North Carolina (Fig. 3a). The rest of the case study domain was essentially cloud free at that time. Most of the stratiform cloud region was free of precipitation although an embedded convective cloud produced a modest amount of rain in southern North Carolina and brief, light showers occurred in western South Carolina and northern Georgia. Otherwise the case was synoptically quiescent. The stratiform clouds dissipated slowly during the morning so that, by early afternoon, they were largely gone (Fig. 3b). During the morning, convective clouds developed in most of the area surrounding the earlier stratiform cloud deck, implying that ground warming and convective destabilization were being locally inhibited by shading in the area covered by stratiform clouds.

The effect of the stratiform clouds on the daytime heating pattern near the surface is apparent in an analysis of the observed change in shelter-height temperatures from 0700 to 1300 EST (Fig. 4). Temperature rises were at a minimum in the area of the stratiform clouds and in the coastal areas affected by the sea breeze. The effect of the cloud-induced shading on the temperature patterns was large and distinct. The local minimum over the North Carolina border was apparently caused by augmentation of the shading effect by evaporative cooling in the rain showers that occurred there.

To satisfy the objectives of the project, six experiments were run, the attributes of which are in Table 2. All of the experiments began at 0700 EST with an upper-air and surface data analysis that used the MM4 objec-

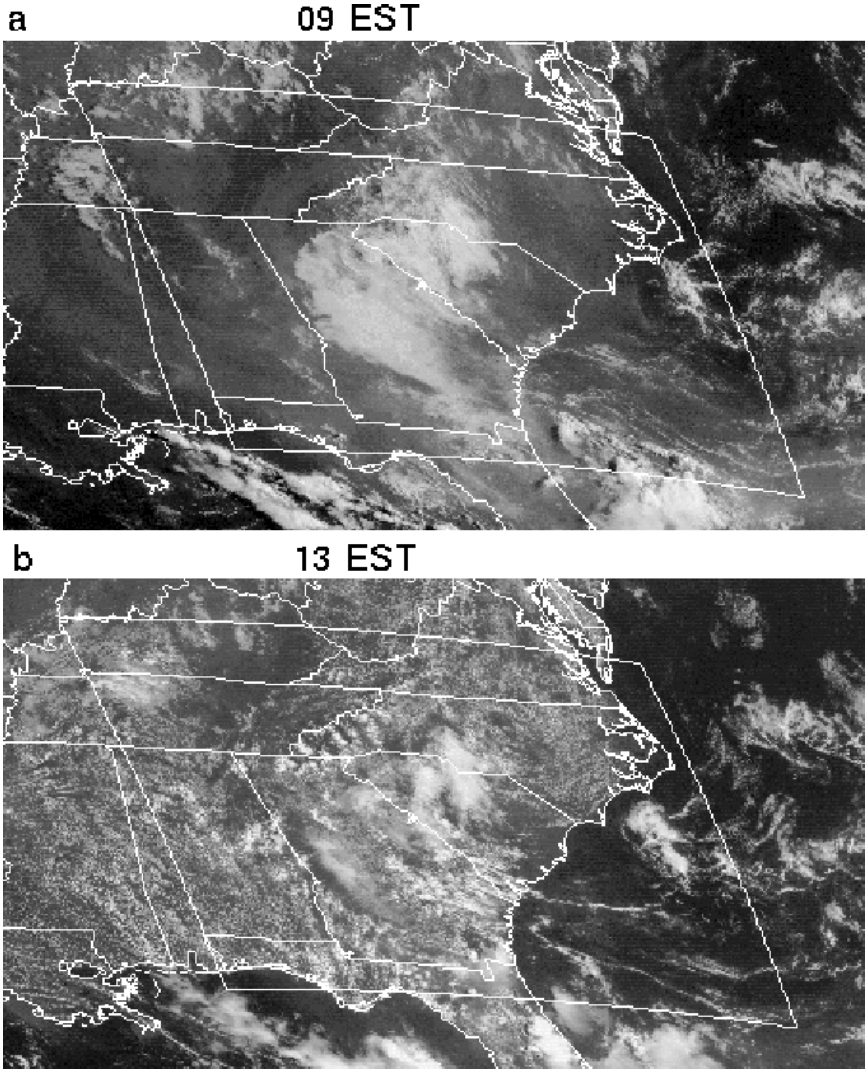

FIG. 3. GOES visible satellite images at (a) 0900 and (b) 1300 EST 23 Aug 1993. The analysis domain is outlined in both frames.

tive analysis package, and the MM4 nonlinear normal-mode adiabatic initialization. Soil temperatures for the domain were determined from an average of analyzed 12-h synoptic-surface temperature values from a 36-h time period around the case study. Initial soil moisture values were the product of climatological moisture availability and surface saturation mixing ratio that is a function of the soil temperature. CON was considered a control run where the MM4 was integrated from 0700 EST with no assimilation after. For SAT, SAT + TEMP, and SAT + ALL, satellite imager data were assimilated once per model time step. For TEMP and SAT + TEMP, the shelter-height temperatures were assimilated at every hour beginning at 0800 EST. For ALL and SAT + ALL all surface observations (surface pressure, shelter-height temperature and relative humidity, and 10-m winds) were assimilated every hour. All six runs continued in assimilation mode until 1300 EST.

The purpose of running experiments in which the shelter-height temperatures were assimilated (TEMP and SAT + TEMP) without the other hourly surface observations was to explore more closely the complementary effects between the shelter-height temperatures and the satellite imager data. The shelter-height temperatures provide information that is closely related to that obtained from the satellite imager. The last two runs (ALL and SAT + ALL) were included for the sake of completeness since the additional surface variables are almost always available in conjunction with the shelter-height temperatures. However, adequately verifying the runs that assimilate the wind fields was not possible since there were no independent data to compare it with.

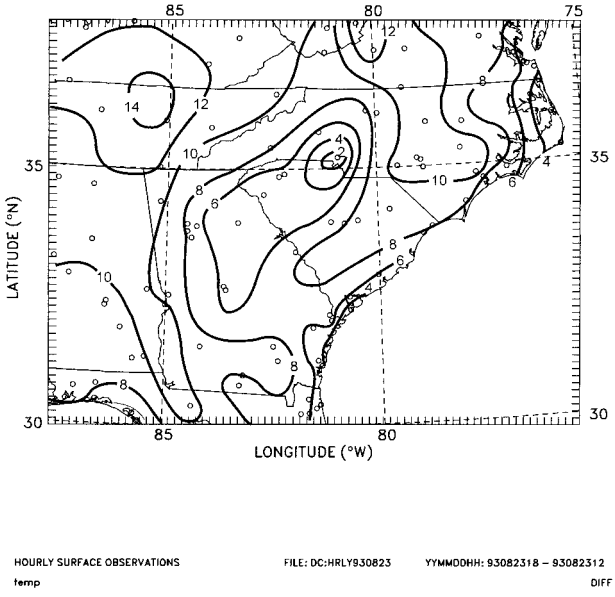

FIG. 4. Change in shelter-height temperature (contoured every 2°C) from 0700 to 1300 EST based on surface observations taken at the stations marked with circles.

Therefore, the results from those runs will not be emphasized.

4. Results

a. Impact of changes to the surface data analysis procedure

Considering that our approach for estimating observation and background error statistics was unconventional, we performed an evaluation of the approach. The values of the estimated observation and background temperature error statistics at each of the six assimilation times are given in Table 3 for the TEMP run. Ideally, the observation error variances should be nearly constant. In this case, the standard deviations (square roots of the variances) stayed within the range from 1.86° to 2.19°C. To determine if the analysis was highly sensitive to the changes in the computed error, the following sensitivity test was carried out. The analysis at 1200 EST for TEMP was rerun using the error statistics computed from the 0800 EST data. These two times were chosen

TABLE 2. Outline of experiments. Variable set (VS) 1 contains satellite imagery; VS 2 contains shelter-height temperature; VS 3 contains shelter-height relative humidity, surface pressure, and 10-m winds.

Experiment	VS 1	VS 2	VS 3
CON			
SAT	X		
TEMP		X	
SAT + TEMP	X	X	
ALL		X	X
SAT + ALL	X	X	X

TABLE 3. Background and observation error standard deviations computed at each analysis time for the TEMP run.

Time (EST)	Background error (°C)	Observation error (°C)
0800	1.68	1.86
0900	1.61	2.02
1000	1.39	2.08
1100	1.46	2.18
1200	1.47	2.19
1300	1.70	1.86

for experimentation because they provided the greatest difference of both the observation error and the ratio of the observation error to background error (i.e., the worst case). This ratio is important in the Bratseth (1986) approach because it determines the degree to which the analysis will fit the observations. The results of the original and rerun analyses were compared. The rms difference between the two analyses for the model's bottom sigma layer temperatures was 0.30°C. For reference the rms difference between the original TEMP analysis and the SAT + TEMP analysis at 1200 EST was 0.46°C. So, even in the worst-case scenario, the sensitivity of the analysis to error specification is less than that derived from different assimilation approaches, although by only a small margin.

Another concern with the revised procedure for assimilating the surface observations was the possible generation of inertia-gravity wave noise by assimilating surface observations without having performed a subsequent initialization to balance the mass and momentum fields. As a way of monitoring the noise in the model, the second derivative with respect to integration time of p^* ($p^* = p_{\text{surface}} - p_{\text{top}}$) was monitored during the experiments (Fig. 5). Each time the surface data were assimilated it caused a shock to the model; however, after each shock the noise rapidly diminished. The analysis shocks from all the assimilated shelter-height and wind observations were equal or greater to the shocks

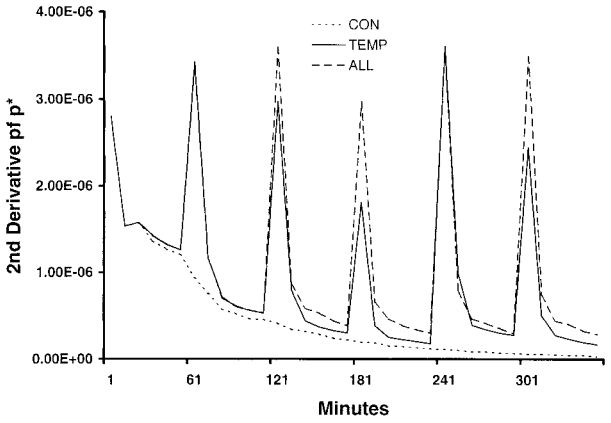

FIG. 5. The second derivative of p^* with respect to integration time (mb s^{-2}) plotted as a function of minutes for the CON, TEMP, and ALL experiments.

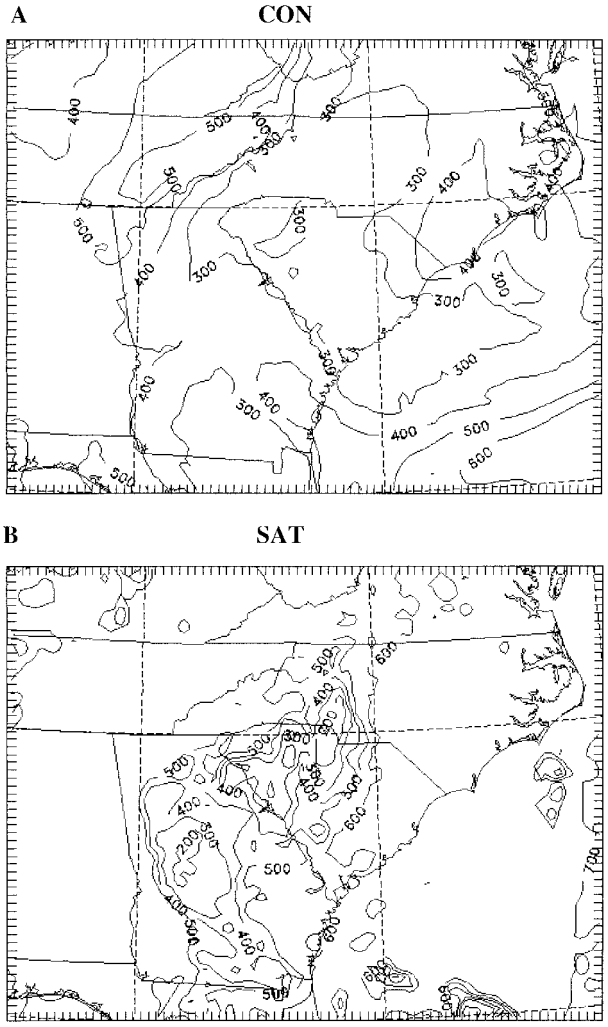

FIG. 6. Surface insolation (W m^{-2}) at 1000 EST from the (a) CON and (b) SAT experiments.

that occurred when assimilating the shelter-height temperatures only. After each of the first three temperature analyses, the second derivative of p^* for TEMP became very close to that for CON. After subsequent temperature assimilation steps, the model did not settle down as much, perhaps due to the increasing mesoscale variability and instability in the atmosphere. The magnitude of the shocks was similar to what the model experienced when beginning integration from the physically balanced initial fields at 0700 EST. To ensure that the presence of these hourly shocks did not produce any adverse effects, the convective precipitation output from the CON and TEMP runs were examined. No spurious convection was evident.

b. Impact of satellite and surface data on thermal analyses

The most immediate and obvious effect of the assimilation of the satellite imager data is to alter the model insolation patterns. The CON insolation field at 1000 EST (Fig. 6) had a broad area with values <300 W m^{-2} and bore little resemblance to the pattern of stratiform cloudiness that persisted through the morning (Fig. 3a). Figure 6 reveals an important source of error that may be introduced by relying on the model's relative humidity field to diagnose cloudiness. The insolation values from SAT, in contrast, were considerably lower in the areas beneath stratiform clouds than in the surrounding areas. The insolation values were larger in SAT than in CON in the area that were shown to be largely clear in the satellite data, particularly in the eastern parts of South Carolina, North Carolina, and Virginia. In the clear areas the SAT results have a gradual east–west gradient, due to the dependence of the local solar angle on longitude (with the sun being east of the domain at this hour).

TABLE 4. Errors in shelter-height temperatures (°C).

	1000 EST		1300 EST	
Experiment	Bias	Rms	Bias	Rms
CON	−0.5	1.7	−1.1	1.9
SAT	0.3	1.4	0.4	1.5
TEMP	−0.5	1.4	−0.2	1.4
SAT + TEMP	−0.1	1.1	0.2	1.2
ALL	−0.2	1.4	−0.2	1.2
SAT + ALL	0.3	1.2	0.4	1.2
Persistence	−1.6	1.8	−0.5	1.1

Shelter-height (2 m) temperatures were computed from the model data in order to assess the impact of the assimilation schemes on the low-level temperatures. The shelter-height temperatures were computed by inverting the model's surface-layer parameterization and were then compared with the observed shelter-height temperatures at 1000 and 1300 EST (Table 4). It is important to note that for the runs that assimilated shelter-height temperature data, the comparisons shown in the table were done before the shelter-height temperatures were assimilated for that particular hour; therefore the evaluations were done on independent data. The CON run for both times exhibited a cold bias that is indicative of the model's inability to properly identify clear areas and produce the appropriate amount of solar heating. Each of the assimilation runs was better than the CON run with respect to both the bias and rms error. To give perspective to the magnitude of the errors in the experiments, error statistics were also computed for persistence. At 1000 EST when a large part of the domain was undergoing diurnal heating, all the experiments improved upon persistence. By 1300 EST the rate of heating had diminished and persistence was slightly better in terms of rms than the assimilation runs. However, all the assimilation runs still showed less bias than persistence.

With regard to the 6-h change in shelter-height temperature (Fig. 7), CON showed no evidence of the cloud shading effect in South Carolina or Georgia (Fig. 3).

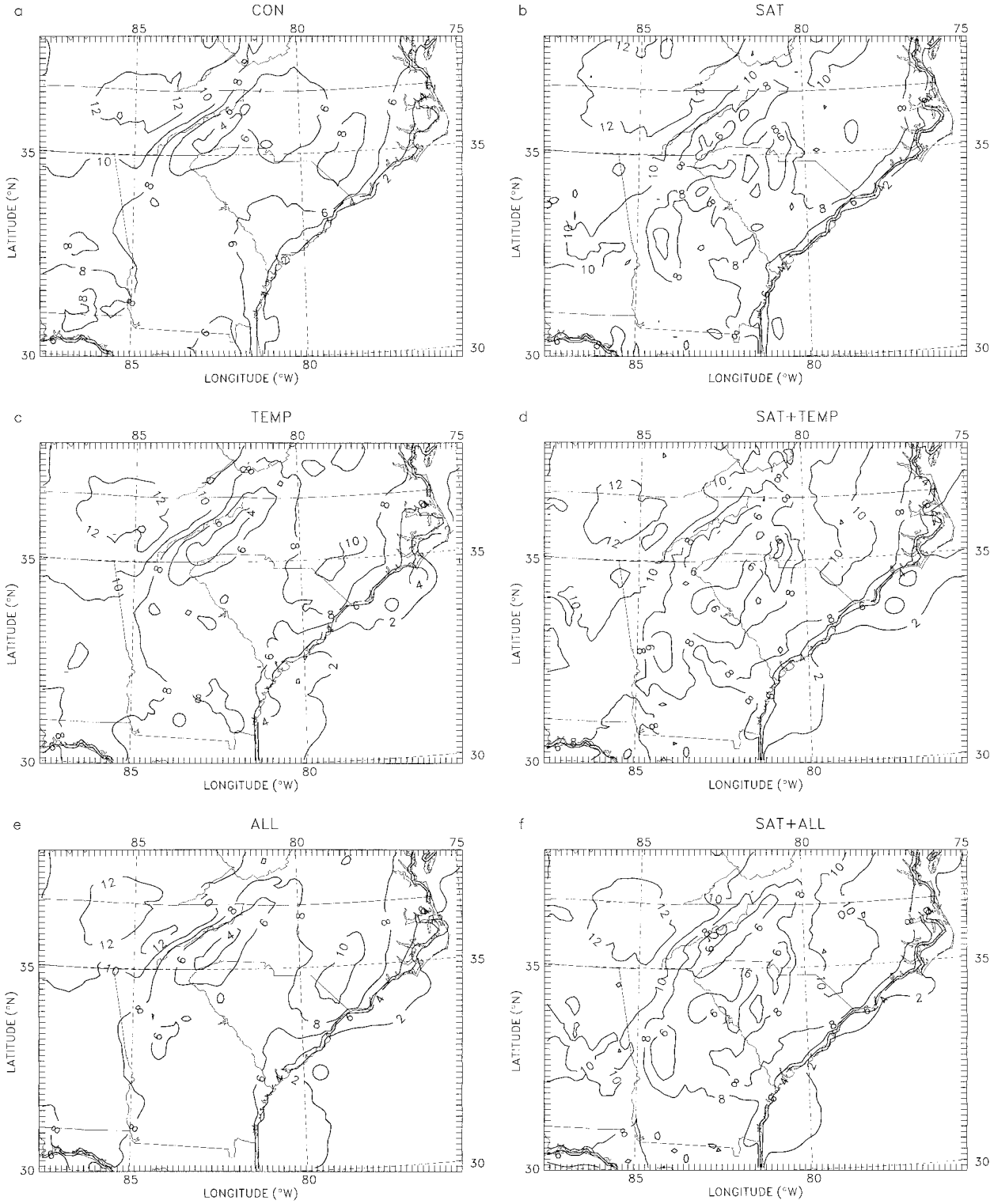

FIG. 7. Change in shelter-height temperature (contoured every 2°C) from 0700 EST to 1300 EST from the (a) CON, (b) SAT, (c) TEMP, (d) SAT + TEMP, (e) ALL, and (f) SAT + ALL experiments.

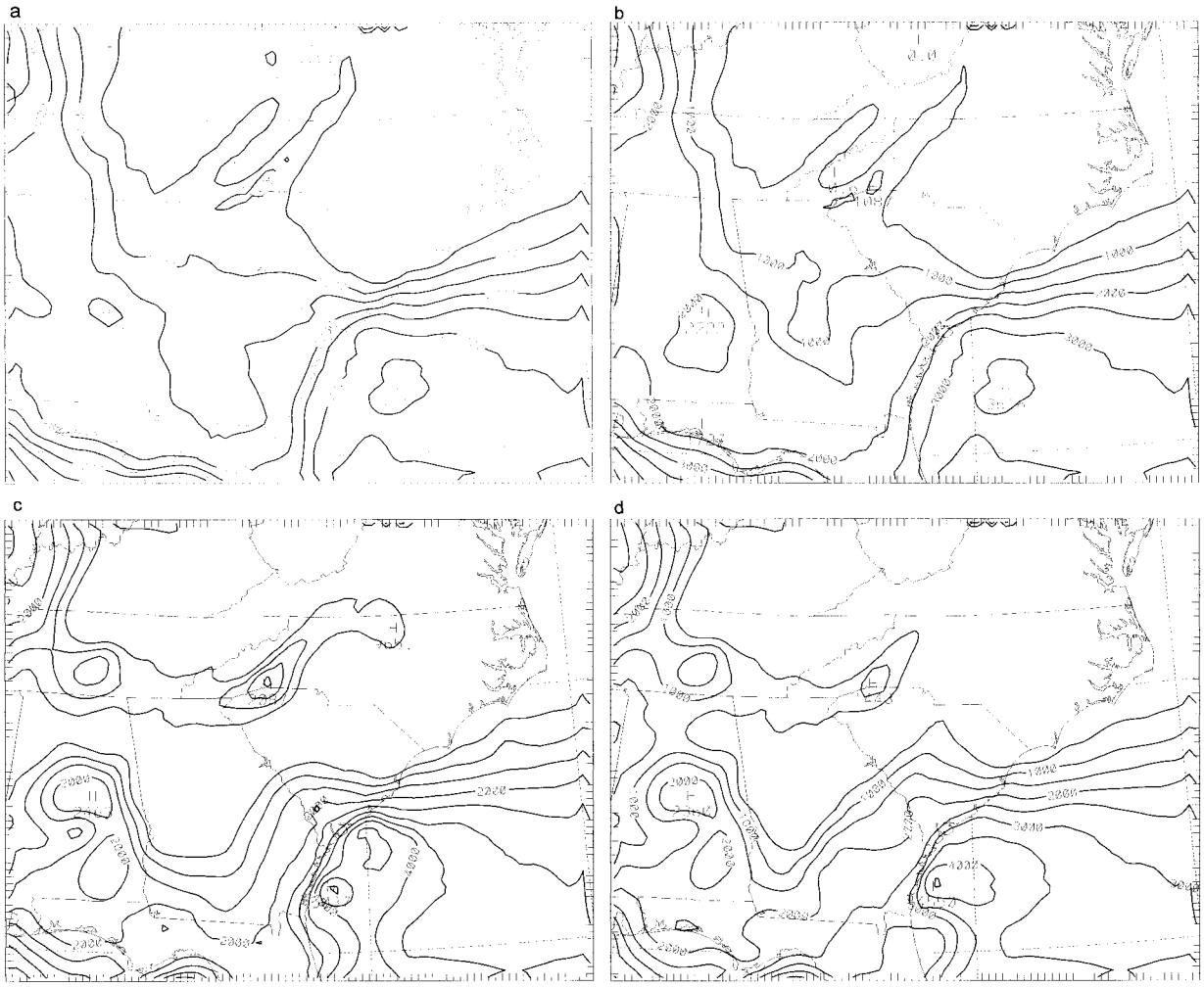

FIG. 8. CAPE values valid at 1000 EST contoured every 500 J kg^{-1} for the (a) CON, (b) SAT, (c) TEMP, and (d) SAT + TEMP experiments.

Conversely, the areas outside the cloud-shaded region did not warm up enough in the CON run. In the SAT run, suppressed warming was apparent in Georgia and South Carolina although this run still warmed the region up a little more than was indicated by the observations. For the unshaded regions, the SAT run did better than the CON run west of the Appalachian Mountains but had temperatures slightly too low in eastern North Carolina. Results from the TEMP run depicted the general warming that occurred outside the cloud-shaded region more accurately than the SAT run, but did not show much improvement relative to the CON run within the shaded region. The SAT + TEMP run was best at revealing the magnitude and the extent of the suppressed warming due to the cloud shading, as well as handling the areas of maximum warming in the clear regions. The lack of any significant shading signature in the ALL results shows that the satellite imager data were still needed to generate the proper level of the thermal effect of the cloud shading.

To assess the utility of the assimilations for analyzing convective potential, the convective available potential energy (CAPE) was computed for the CON, SAT, TEMP, and SAT + TEMP results valid at 1000 EST (Fig. 8). All four runs showed a region of values >2000 J kg^{-1} in Alabama, which matched up well with the convection seen in the area by 1300 EST (Fig. 3b) and which intensified into the evening. However, only the runs that assimilated the shelter-height temperature fields showed a minimum of CAPE of <500 J kg^{-1} associated with the shaded region. While convection may be suppressed even in areas with high values of CAPE, this result is consistent with the lack of convection noted in the shaded region at 1300 EST.

c. *Impact of satellite and shelter-height temperature data on wind fields*

The lowest level (σ = 0.995) wind fields for the six experiments were objectively compared with the ob-

TABLE 5. Rms of the magnitude of the wind error vector (m s^{-1}) with respect to the observed 10-m winds.

Experiment	1000 EST	1300 EST
CON	3.23	3.53
SAT	3.18	3.48
TEMP	3.15	3.38
SAT + TEMP	3.14	3.38
ALL	3.12	3.21
SAT + ALL	3.11	3.21

served 10-m winds to determine if the wind field adjusted to the perturbations in the mass field that came about through assimilation. The rms errors of the magnitude of the wind error vectors are presented in Table 5. As was done with the temperature error statistics, the wind errors were computed at a particular hour were calculated prior to the analysis at that hour for the runs that assimilated winds. The results show improvement with respect to the CON run for all the assimilation runs, but it is apparent that the assimilation of the shelter-height temperatures contributed marginally more improvement over the assimilation of the satellite imager data. The reason is because the vertical blending of the surface analysis increments in the TEMP run results in a deeper layer of temperature adjustments than when only improving the surface computation in the SAT run.

The horizontal mass divergence fields valid at 1300 EST (Fig. 9) were considered because of their sensitivity to changes in mesoscale circulations and their association with convective development. For the ALL and SAT + ALL runs, the divergence fields were computed prior to the analysis of the 1300 EST wind observations. The CON run had very low divergence magnitudes except for features produced by orography in the Appalachian Mountains of North Carolina and Virginia. The other three experiments depicted convergence along the Alabama–Georgia border that was in the vicinity of developing convection (Fig. 3b). The SAT and SAT + TEMP runs depicted convergence that was correlated with developing convection in southern South Carolina and southeastern Georgia and depicted a band of divergence in the shaded area of western Georgia. The divergence plots for the ALL and SAT + ALL runs indicate that the assimilation of the winds through hourly analysis updates did not impede the development of the model divergence. In fact, the SAT + ALL run had the strongest convergence intensities of all the runs for the area along the Alabama–Georgia border. While it is impossible to verify directly this result, it was consistent with the convective clouds that were observed to develop (Fig. 3b) and intensify in that area, producing level 4 radar echoes in manually digitized radar data (not shown).

The effect of the satellite imager data and shelter-height temperature assimilation on mesoscale circulations is illustrated in Fig. 10 by cross sections valid at 1300 EST. All three assimilation runs depicted moisture divergence at low levels in the stratiform cloud area and moisture convergence on the adjoining sides. The SAT and SAT + TEMP runs had greater magnitudes of divergence and convergence than did the TEMP run. The CON run showed very little divergence or convergence. The assimilation runs produced a slightly stronger sea breeze circulation, as evident by the stronger onshore flow, and a stronger updraft over the high ground to the northwest of the cloudy area, in comparison with the CON run. The assimilation runs that included the satellite imager data produced suppressed boundary layer development over the stratiform cloud area. All the assimilation runs displayed enhanced boundary layer development on each side of the cloudy region. The collapse of the boundary layer near the coast for the TEMP run is noteworthy. The assimilation of the shelter-height temperature and satellite imagery data result in warmer lower-tropospheric and ground temperatures, respectively, in this area for the SAT + TEMP run compared to the control run. The result is that the surface heat flux is not significantly altered. However in the TEMP run, only the lower-tropospheric temperature is raised in this area. The result is that, with a strong horizontal ground temperature gradient across the coast, there is an area just offshore where a stable or nearly stable surface layer is created. In these types of stability regimes, the MM4 sets the boundary layer height to zero. The boundary layer height depictions illustrate a potential pitfall when assimilating single-layer data. However, it also shows how combining two independent sources of data can mitigate the limitations of the individual sources.

5. Conclusions

It is obvious from our results that the MM4, on its own, cannot accurately reproduce many important low-level perturbations caused by the cloud shading. This shortcoming is most pronounced in the absence of strong synoptic forcing such as the case presented here. It is certainly not the purpose of this paper to single out the MM4 for criticism in this regard. Other widely used mesoscale models, including some that include explicit clouds (e.g., Grell et al. 1995; Hodur 1997), use similar cloud parameterizations for shortwave radiation as the MM4. The main problem with the current model parameterization in the case presented here is that it relies on relative humidity to diagnose clouds and the relative humidity is not well correlated with the actual cloud cover. The result is that the MM4 did not infer the correct amount of downward solar radiation, so in regions that were actually clear it did not allow sufficient solar radiation to reach the ground, leading to a cool bias of computed shelter-height temperatures and a lack of appropriate mesoscale detail. Without the production of the cloud shading thermal effects, little prior indication of convective activity is given by the MM4 without assimilation. The assimilation of the satellite imager

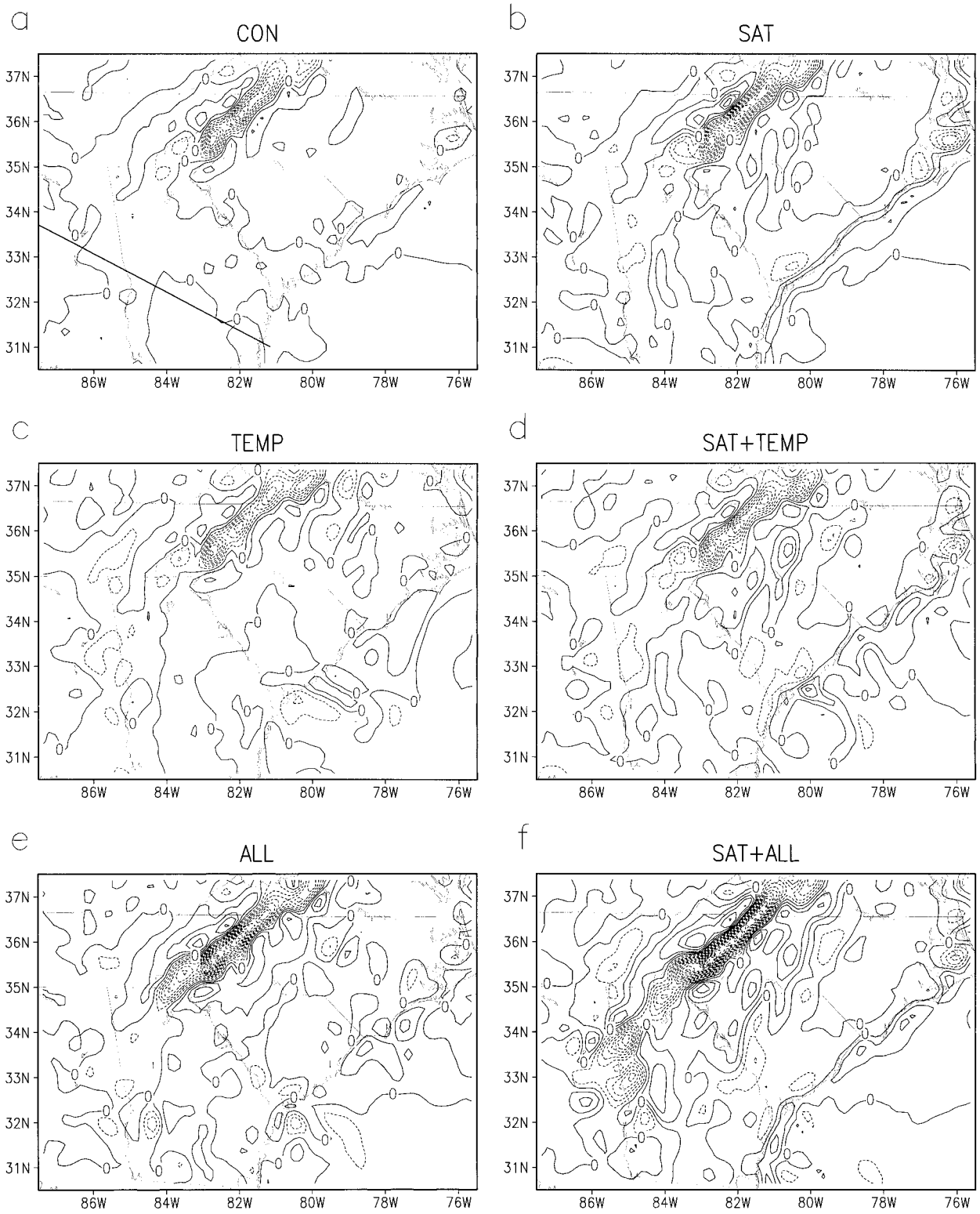

FIG. 9. Divergence at 1300 EST for the model's lowest level ($\sigma = 0.995$) from the (a) CON, (b) SAT, (c) TEMP, (d) SAT + TEMP, (e) ALL, and (f) SAT + ALL experiments. The contour interval is 3×10^{-5} s^{-1} with negative contours dashed. The solid line in (a) depicts the location of cross sections in Fig. 10.

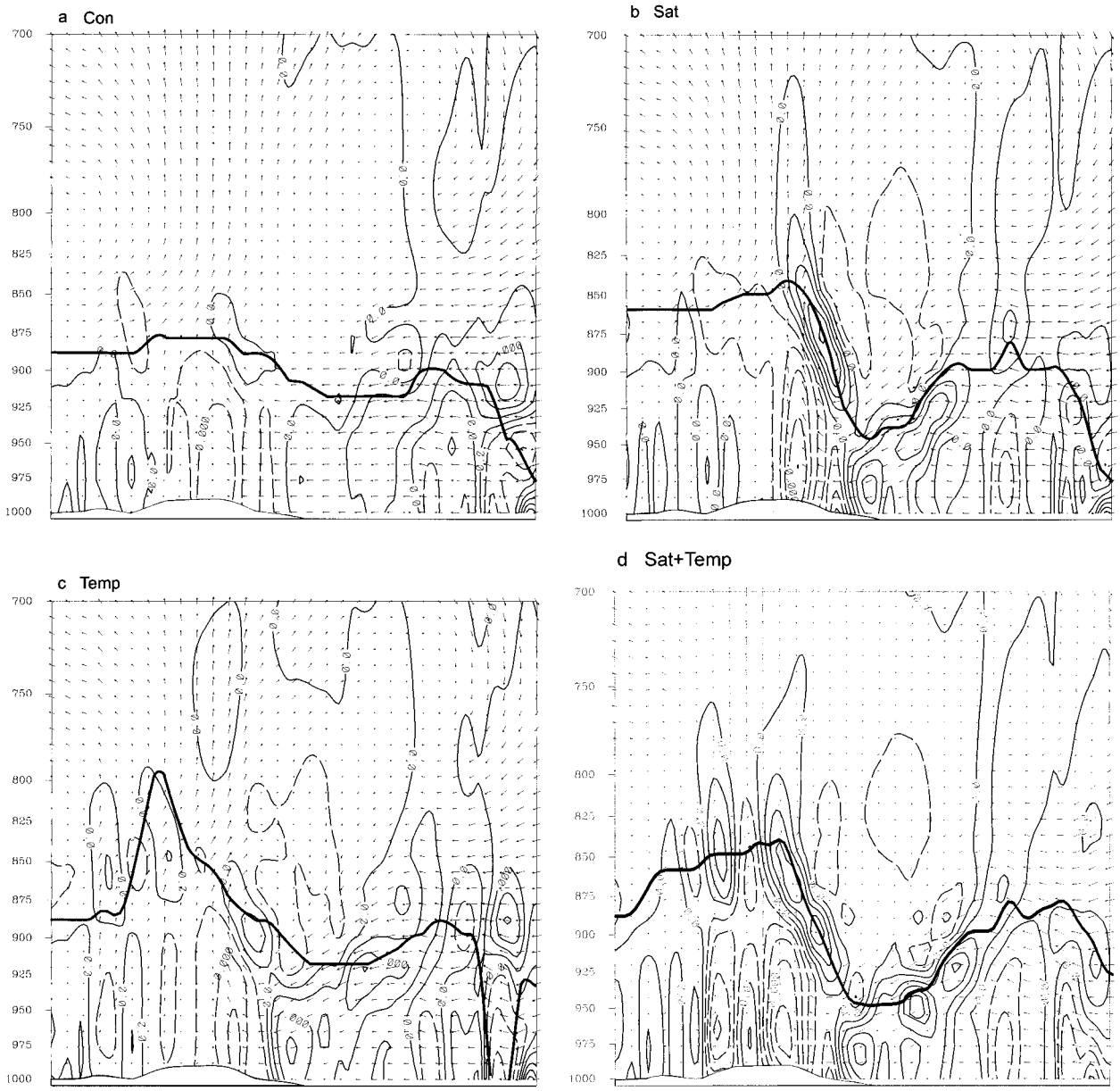

FIG. 10. Cross sections of wind and moisture divergence at 1300 EST from the (a) CON, (b) SAT, (c) TEMP, and (d) SAT + TEMP experiments. The cross sections go from northwest (left) to southeast (right) along the line shown in Fig. 9a. The contour interval is 2×10^{-7} s^{-1}, with the negative contours dashed. The vector scaling is 6 m s^{-1} and 0.6 Pa s^{-1} per vector interval in the horizontal and vertical directions, respectively. The heavy solid line marks the top of the boundary layer.

data improved the representation of the surface insolation and thus does a better job of representing the shelter-height temperatures. However, in the region affected by the cloud shading the suppression of shelter-height temperatures was greater in the observations than in the assimilation analyses. This underrepresentation possibly could be rooted in the retrievals of τ_{eff}, although no ground-truth data were available. Retrieved values of τ_{eff} were <0.4 over most of the cloud-covered area, and substantial areas had values <0.3. A more likely source of error was the model's surface energy budget, which is susceptible to errors caused by latent heat flux uncertainties. As mentioned earlier, we were unable to use retrieved ground surface temperatures from the infrared sounder as part of the satellite assimilation procedure. Our results suggest that ground surface temperature assimilation would not have had a significant beneficial impact on the experiments, since this data would have been available only in cloud-free areas—the very same region where the analysis did well.

Assimilation of the shelter-height temperatures—without the satellite imager data—provided a better de-

piction of low-level temperature than the control run; however, the fields from the assimilation of shelter-height temperatures lacked the level of spatial detail that was present after assimilating the satellite imager data. This is not unexpected since the horizontal spatial resolution of the surface observations is substantially coarser than that available from the satellite imager. The shelter-height temperature assimilation, on its own, did not completely represent the shading effect. This further illustrates the problem noted above that, while we are partly improving the low-level temperature representation, we are not producing the accurate surface heat flux.

Complementary improvement in several model variables was evident during assimilation of both the satellite imager and the shelter-height temperature data. There was an improved depiction of the shelter-height temperatures for the combined assimilation of satellite imager data and shelter-height temperatures, as compared to the runs that assimilated the sources separately. The combined assimilation run also produced more realistic divergence fields and indices of potential for convective cloud development, as evaluated by consistency with observed patterns of cloud development.

The assimilation of shelter-height temperature, in particular, improved the model depiction of the wind field. This effect is apparent in the magnitude of the wind error vectors as well as in the divergence fields. When 10-m wind data were assimilated intermittently, there were no persistent harmful effects to the model-generated divergence fields.

We have not presented forecasts generated from the combined assimilation because the effect of the satellite imager assimilation is quickly lost during the forecast as the model reverts back to its own way of parameterizing clouds for surface insolation computations. If one desired to continue to estimate the surface insolation more realistically in forecast mode it would be necessary to adjust the model relative humidities. Lipton and Modica (1999) have reported on such a method that enforces consistency with satellite cloud observations. We also note here that this work focused on the radiative effects of stratiform clouds. Under certain conditions, the dynamic effects of convective clouds can also be important. Others (e.g., Puri and Miller 1990; Harms et al. 1993) have addressed the use of satellite data to constrain a model's convective dynamics. Ultimately it would be wise for mesoscale models to incorporate both kinds of assimilation.

The analysis system that is described here for combining satellite imager and surface observation data has demonstrated potential for local-scale analysis of convective initiation. In addition, the system is relatively efficient computationally. Therefore it is feasible that, pending further testing and evaluation, the system could be deployed at local forecast offices as an aid in the nowcasting of convective initiation. Indeed, the techniques discussed here can be adapted to many of the mesoscale models already run at local forecast centers.

Acknowledgments. We thank T. Stoffel of the National Renewable Energy Laboratory for providing the pyranometer data and D. C. Peduzzi and G. B. Gustafson of Atmospheric and Environmental Research, Inc. for writing the cloud-clear discrimination program for satellite imagery. In addition, we thank T. Walker for assistance in preparing figures. Surface weather observation data were provided by the USAF Combat Climatology Center. This research was supported in part by the Air Force Office of Scientific Research under project 2310 and by the Department of Defense High Performance Computing Shared Resource Centers at the Army Corps of Engineers Waterways Experiment Station and at the Naval Oceanographic Office.

REFERENCES

Abbs, D. J., and R. A. Pielke, 1986: Thermally forced surface flow and convergence patterns over northeast Colorado. *Mon. Wea. Rev.,* **114,** 2281–2296.

Anthes, R. A., 1977: A cumulus parameterization scheme utilizing a one-dimensional cloud model. *Mon. Wea. Rev.,* **105,** 270–286.

Bailey, M. J., K. M. Carpenter, L. R. Lowther, and C. W. Passant, 1981: A mesoscale forecast for 14 August 1975—The Hampstead storm. *Meteor. Mag.,* **110,** 147–161.

Benjamin, S. G., 1983: Some effects of surface heating and topography on the regional severe storm environment. Ph.D. dissertation, The Pennsylvania State University, 265 pp. [Available from The Pennsylvania State University, University Park, PA 16802.]

——, and N. L. Seaman, 1985: A simple scheme for objective analysis in curved flow. *Mon. Wea. Rev.,* **113,** 1184–1198.

Blackadar, A. K., 1979: High-resolution models of the planetary boundary layer. *Advances in Environmental Science and Engineering,* J. Pfafflin and E. Ziegler, Eds., Vol. 1, No. 1, Gordon and Breach, 50–85.

Bratseth, A. M., 1986: Statistical interpolation by means of successive corrections. *Tellus,* **38A,** 439–447.

Burpee, R. W., 1979: Peninsula-scale convergence in the south Florida sea breeze. *Mon. Wea. Rev.,* **107,** 852–860.

Byers, H. R., and R. R. Braham Jr., 1949: *The Thunderstorm.* U.S. Government Printing Office, 287 pp.

Daley, R., 1991: *Atmospheric Data Analysis.* Cambridge University Press, 457 pp.

Diak, G. R., and C. Gautier, 1983: Improvements to a simple physical model for estimating insolation from GOES data. *J. Climate Appl. Meteor.,* **22,** 505–508.

Errico, R. M., and G. T. Bates, 1988: Implicit normal-mode initialization of the PSU/NCAR mesoscale model. NCAR Tech. Note NCAR T/N-312 + IA, 112 pp. [Available from NCAR Information Services, P.O. Box 3000, Boulder, CO 80307.]

Gautier, C., G. Diak, and S. Masse, 1980: A simple physical model to estimate incident solar radiation at the surface from GOES satellite data. *J. Appl. Meteor.,* **19,** 1005–1012.

Grell, G. A., J. Duhia, and D. R. Stauffer, 1995: A description of the fifth generation Penn State/NCAR Mesoscale Model (MM5). NCAR Tech. Note NCAR T/N-398 + STR, 122 pp. [Available from NCAR Information Services, P.O. Box 3000, Boulder, CO 80307.]

Hanson, K., and T. Stoffel, 1989: Solar radiation monitor networks. *Solar Resources,* R. L. Hulstrom, Ed., The MIT Press, 143–171.

Harms, D. E., R. V. Madala, S. Raman, and K. D. Sashegyi, 1993: Diabatic initialization tests using the Naval Research Laboratory

limited-area numerical weather prediction model. *Mon. Wea. Rev.*, **121,** 3184–3190.
Hodur, R. M., 1997: The Naval Research Laboratory's Coupled Ocean/Atmosphere Mesoscale Prediction System (COAMPS). *Mon. Wea. Rev.*, **125,** 1414–1430.
Hong, X., M. J. Leach, and S. Raman, 1995: A sensitivity study of convective cloud formation by vegetative forcing with different atmospheric conditions. *J. Appl. Meteor.*, **34,** 2008–2028.
Lipton, A. E., 1993: Cloud shading retrieval and assimilation in a satellite-model coupled mesoscale analysis system. *Mon. Wea. Rev.*, **121,** 3062–3081.
——, and T. H. Vonder Haar, 1990: Mesoscale analysis by numerical modeling coupled with sounding retrieval from satellites. *Mon. Wea. Rev.*, **118,** 1308–1329.
——, and G. D. Modica, 1999: Assimilation of visible-band satellite data for mesoscale forecasting in cloudy conditions. *Mon. Wea. Rev.*, **127,** 265–278.
——, ——, S. T. Heckman, and A. J. Jackson, 1995: Satellite-model coupled analysis of convective potential in Florida with VAS water vapor and surface temperature data. *Mon. Wea. Rev.*, **123,** 3292–3304.
McNider, R. T., J. A. Song, and S. Q. Kidder, 1995: Assimilation of GOES-derived solar insolation into a mesoscale model for studies of cloud shading effects. *Int. J. Remote Sens.*, **16,** 2207–2231.
Menzel, W. P., and J. F. W. Purdom, 1994: Introducing GOES-I: The first of a new generation of geostationary operational environmental satellites. *Bull. Amer. Meteor. Soc.*, **75,** 757–781.
Method, T. J., and T. N. Carlson, 1982: Radiative heating rates and some optical properties of the St. Louis aerosol, as inferred from aircraft measurements. *Atmos. Environ.*, **16,** 53–66.
Miller, P. A., and S. G. Benjamin, 1992: A system for the hourly assimilation of surface observations in mountainous and flat terrain. *Mon. Wea. Rev.*, **120,** 2342–2359.
Peterson, J. T., E. C. Flowers, G. J. Berri, C. L. Reynolds, and J. H. Rudisill, 1981: Atmospheric turbidity over central North Carolina. *J. Appl. Meteor.*, **20,** 229–241.
Purdom, J. F. W., and K. Marcus, 1982: Thunderstorm trigger mechanisms over the southeast United States. Preprints, *12th Conf. on Severe Local Storms,* San Antonio, TX, Amer. Meteor. Soc., 487–488.
Puri, K., and M. J. Miller, 1990: The use of satellite data in the specification of convective heating for diabatic initialization and moisture adjustment in numerical weather prediction models. *Mon. Wea. Rev.*, **118,** 67–93.
Rabin, R. M., S. Stadler, P. J. Wetzel, D. J. Stensrud, and M. Gregory, 1990: Observed effects of landscape variability on convective clouds. *Bull. Amer. Meteor. Soc.*, **71,** 272–280.
Ruggiero, F. H., K. D. Sashegyi, R. V. Madala, and S. Raman, 1996: The use of surface observations in four-dimensional data assimilation using a mesoscale model. *Mon. Wea. Rev.*, **124,** 1018–1033.
Schmetz, J., 1989: Towards a surface radiation climatology: Retrieval of downward irradiances from satellites. *Atmos. Res.*, **23,** 287–321.
Segal, M., J. F. W. Purdom, J. L. Song, R. A. Pielke, and Y. Mahrer, 1986: Evaluation of cloud shading effects on the generation and modification of mesoscale circulations. *Mon. Wea. Rev.*, **114,** 1201–1212.
——, W. L. Physick, J. E. Heim, and R. W. Arritt, 1993: The enhancement of cold-front temperature contrast by differential cloud cover. *Mon. Wea. Rev.*, **121,** 867–873.
Stephens, G. L., 1978: Radiation profiles in extended water clouds. Part II: Parameterization schemes. *J. Atmos. Sci.*, **35,** 2123–2132.
——, S. Ackerman, and E. A. Smith, 1984: A shortwave parameterization revised to improve cloud absorption. *J. Atmos. Sci.*, **41,** 687–690.
Toth, J. J., and R. H. Johnson, 1985: Summer surface flow characteristics over northeast Colorado. *Mon. Wea. Rev.*, **113,** 1448–1469.
Weinreb, M. P., R. Xie, J. H. Lienesch, and D. S. Crosby, 1989: Destriping GOES images by matching empirical distribution functions. *Remote Sens. Environ.*, **29,** 185–195.
Zhang, D., and R. A. Anthes, 1982: A high-resolution model of the planetary boundary layer—Sensitivity tests and comparisons with SESAME-79 data. *J. Appl. Meteor.*, **21,** 1594–1609.